Proteomics of Genetically Engineered Mouse Mammary Tumors Identifies Fatty Acid Metabolism Members as Potential Predictive Markers for Cisplatin Resistance*

Marc Warmoes‡§, Janneke E. Jaspers§¶‖, Guotai Xu¶, Bharath K. Sampadi‡¶, Thang V. Pham‡, Jaco C. Knol‡, Sander R. Piersma‡, Epie Boven‡, Jos Jonkers‖, Sven Rottenberg¶‡‡, and Connie R. Jimenez‡§§**

In contrast to various signatures that predict the prognosis of breast cancer patients, markers that predict chemotherapy response are still elusive. To detect such predictive biomarkers, we investigated early changes in protein expression using two mouse models for distinct breast cancer subtypes who have a differential knock-out status for the breast cancer 1, early onset (*Brca1*) gene. The proteome of cisplatin-sensitive BRCA1-deficient mammary tumors was compared with that of cisplatin-resistant mammary tumors resembling pleomorphic invasive lobular carcinoma. The analyses were performed 24 h after administration of the maximum tolerable dose of cisplatin. At this time point, drug-sensitive BRCA1-deficient tumors showed DNA damage, but cells were largely viable. By applying paired statistics and quantitative filtering, we identified highly discriminatory markers for the sensitive and resistant model. Proteins up-regulated in the sensitive model are involved in centrosome organization, chromosome condensation, homology-directed DNA repair, and nucleotide metabolism. Major discriminatory markers that were up-regulated in the resistant model were predominantly involved in fatty acid metabolism, such as fatty-acid synthase. Specific inhibition of fatty-acid synthase sensitized resistant cells to cisplatin. Our data suggest that exploring the functional link between the DNA damage response and cancer metabolism shortly after the initial treatment may be a useful strategy to predict the efficacy of cisplatin. ***Molecular & Cellular Proteomics 12: 10.1074/mcp.M112.024182, 1319–1334, 2013.***

From the ‡OncoProteomics Laboratory, Department of Medical Oncology, VU University Medical Center, De Boelelaan 1117, 1081HV Amsterdam and the ¶Division of Molecular Oncology and ‖Division of Molecular Pathology, Netherlands Cancer Institute, Plesmanlaan 121 Amsterdam, 1066 CX, The Netherlands

Received September 19, 2012, and in revised form, January 31, 2013

Published, MCP Papers in Press, February 8, 2013, DOI 10.1074/mcp.M112.024182

Breast cancer is a heterogeneous disease consisting of a variety of subtypes that need different treatment strategies. In contrast to several prognostic signatures for clinical outcome, markers that predict treatment efficacy have been difficult to define. Reasons to explain this failure have been discussed elsewhere (1). A shortcoming of previous attempts to identify such markers may be that tumors were usually not challenged by drugs when sampled for analysis, or treatment was given a few weeks before sampling (neoadjuvant trials). Moreover, most previous studies focused on the analysis of gene expression to identify useful markers. However, differential expression of relevant factors, such as those involved in the DNA damage response, may be easier to detect shortly after chemotherapy-induced stress, and protein level readouts may provide a more direct way of assessing drug response.

In this study, we aimed at detecting predictive biomarkers at the protein level by comparing the short term treatment response of platinum-sensitive *versus* platinum-resistant mouse mammary tumors that represent different breast cancer subtypes. As a sensitive model, we used the *K14cre*;*Brca1*$^{F/F}$;*p53*$^{F/F}$ mouse model (2) for BRCA1[1]-deficient breast cancer. The *Brca1*$^{-/-}$;*p53*$^{-/-}$ tumors that arise in this model include a large intragenic deletion of *Brca1*, and we have previously shown that these tumors are highly sensitive to cisplatin treatment (3). The response that we observed in this mouse model is consistent with the sensitivity of BRCA1-like breast cancer to intensive platinum-based chemotherapy in the clinic (4). Moreover, it was recently shown that triple-negative breast cancer patients frequently respond to cisplatin treatment, especially in patients with lower BRCA1 expression (5).

As resistant model, we chose *WAPcre*;*Cdh1*$^{F/F}$;*p53*$^{F/F}$ mice. The cadherin-1 (CDH1)- and p53-deficient mammary

[1] The abbreviations used are: BRCA1, breast cancer antigen 1; FASN, fatty-acid synthase; CDH1, cadherin-1; PARP1, poly(ADP-ribose) polymerase 1; HR, homologous recombination; p53, tumor protein p53; BisTris, 2-[bis(2-hydroxyethyl)amino]-2-(hydroxymethyl)-propane-1,3-diol; PPAR, peroxisome proliferator-activated receptor.

tumors generated in these animals resemble human pleomorphic invasive lobular carcinomas (6). We show here that the tumors of this model hardly respond to cisplatin. This is also consistent with the nature of invasive lobular carcinoma cancers in patients, which usually have only a modest benefit of chemotherapy as compared with invasive ductal carcinoma (7).

Platinum agents induce DNA damage by forming inter- and intrastrand DNA cross-links. The repair of DNA-platinum adducts involves several repair pathways including the Fanconi anemia pathway, nucleotide excision repair, and homologous recombination (HR) (8). Because BRCA1 is an important player in the HR pathway, which results in error-free repair of double strand breaks, it is not unexpected that BRCA1-deficient tumors respond to platinum. Multiple cisplatin resistance mechanisms have been put forward (9), of which reactivation of the HR pathway by genetic restoration of BRCA1 function is found to be a clinically relevant cisplatin resistance mechanism (10).

Unfortunately, the precise BRCA1 status or HR activity of tumor cells is frequently not known for breast cancer patients. Early treatment resistance and response proteins that assess HR competence, both in familial and sporadic breast cancers, could therefore aid in selecting patients for platinum-based chemotherapy. In addition, identification of (druggable) predictive markers of resistant tumors might help to identify patients that need an alternative treatment.

In this study, we found that major discriminatory proteins after treatment with cisplatin are involved in fatty acid metabolism and signaling. These proteins include the following: FASN, which is known as a central player in *de novo* fatty acid synthesis; fatty acid-binding protein 4 (FABP4), a major transporter of fatty acids; and γ-synuclein, a protein that has hypothesized lipid binding properties. Our data suggest that the analysis of fatty acid metabolism may be a useful readout to predict platinum resistance early after initial treatment.

EXPERIMENTAL PROCEDURES

Materials

All chemicals, unless otherwise specified, were obtained from Sigma-Aldrich. HPLC solvents, LC-MS grade water, acetonitrile, and formic acid were obtained from Biosolve (Biosolve B.V., Valkenswaard, The Netherlands). Porcine sequence-grade modified trypsin was obtained from Promega (Promega Benelux B.V., Leiden, The Netherlands).

Mouse Tumors

The generation of *Cdh1*$^{-/-}$;*p53*$^{-/-}$(WEP) or *Brca1*$^{-/-}$;*p53*$^{-/-}$ (KB1P) mammary tumors has been described previously (2, 6, 11). Orthotopic transplantation of tumors into syngeneic mice and treatment with cisplatin were performed as reported previously (3). Tumor samples for the proteomic analysis were snap-frozen and stored at −80°C until use. All animal experiments were approved by The Netherlands Cancer Institute ethical review committee.

Cell Culture and RNA Interference

The *Cdh1*$^{-/-}$;*p53*$^{-/-}$ cell line (KEP11) was derived from a primary tumor that arose in a *K14cre*;*Cdh1*$^{F/F}$;*Trp53*$^{F/F}$ mouse, and the cells were cultured as described (11). KEP11 cells were transduced with pLKO-puro short hairpin RNA (shRNA) lentiviruses obtained from Mission library clones (Sigma-Aldrich). To target *Fasn*, we used TRCN0000075704 (shRNA#1) and TRCN0000075707 (shRNA#2). After selection with 3 μg/ml puromycin, 8000 cells per well were seeded in 6-well plates and assayed for clonal growth in the presence of cisplatin. 1 day after seeding, cells were incubated for 24 h with 2, 2.25, or 2.5 μM cisplatin. Surviving colonies were visualized using Leishman stain 6, 8, or 9 days after starting treatment.

The efficacy of *Fasn* inhibition was determined by quantitative RT-PCR using the LightCycler® 480 SYBR Green I Master reagents according to the manufacturer's protocol (Roche Applied Science, catalog number 4707516001). To amplify mouse hypoxanthine-guanine phosphoribosyltransferase *Hprt* or *Fasn* cDNA, the following primers were used (5′ to 3′): Hprt_for (CTGGTGAAAAGGACCTCTCG) and Hprt_rev (TGAAGTACTCATTATAGTCAAGGGCA); Fasn_for (ATTGTCGCTCTGAGGCTGTTG) and Fasn_rev (TTGCTCCTTGCTGCCATCTG). To measure cell proliferation, ~2000 KEP11-derived cells were seeded into 96-well plates. At the indicated time points, each well was refreshed by 150 μl of fresh medium containing 3-(4,5-dimethylthiazol-2-yl)-2,5-diphenyltetrazolium bromide (0.5 mg/ml, Sigma-Aldrich) and incubated for another 4 h at 37°C. Then the medium was removed, and 150 μl of DMSO was added into each well to dissolve the resultant formazan crystals. Cell growth was determined by the absorbance detected at 490 nm using a microplate reader (Tecan, Infinite M200PRO).

Tissue Homogenization and Fractionation Using Gel Electrophoresis

For homogenization, we cut into smaller parts an ~20-mg piece of tumor tissue into a bath of liquid nitrogen. The proteins in the breast tumor tissue samples were solubilized in 800 μl of 1× reducing SDS Sample Buffer (containing 62.5 mM Tris-HCl, 2% w/v SDS, 10% v/v glycerol, and 0.0025% bromphenol blue, 100 mM DDT, pH 6.8) using a Pellet Pestles micro-grinder system (Kontes Glassware, Vineland, NJ). Subsequently, the proteins were denatured by heating at 100°C for 10 min. Any insoluble debris was removed by centrifugation for 15 min at maximum speed (16.1 relative central force) in a bench top centrifuge.

Proteins were fractionated using one-dimensional SDS-PAGE. 25 μl of each homogenized sample (containing about 50 μg of protein) was loaded into a well of a pre-cast 4–12% NuPAGE (w/v) BisTris 1.5-mm minigel (Invitrogen). The stacking gel contained 4% (w/v) acrylamide/BisTris. Electrophoresis was carried out at 200 V in NuPAGE MES SDS running buffer (50 mM Tris base, 50 mM MES, 0.1% w/v SDS, 1 mM EDTA, pH 7.3) until the dye front reached the end of the gel. Following electrophoresis, gels were fixed with a solution of 50% ethanol and 3% phosphoric acid. Staining was carried out in a solution of 34% methanol, 3% phosphoric acid, 15% ammonium sulfate, and 0.1% Coomassie Blue G-250 (Bio-Rad) with subsequent destaining in milli-Q water.

In-gel Digestion and Nano-liquid Chromatography-Fourier Transformation-Mass Spectrometry (nanoLC-FT-MS)

In-gel digestion and nanoLC-FT-MS for the 12 tumors from the discovery experiment were performed as described previously (12). In short, processed gel lanes were cut in 10 equal bands, after which they were in-gel digested with trypsin. Extracted peptides from each

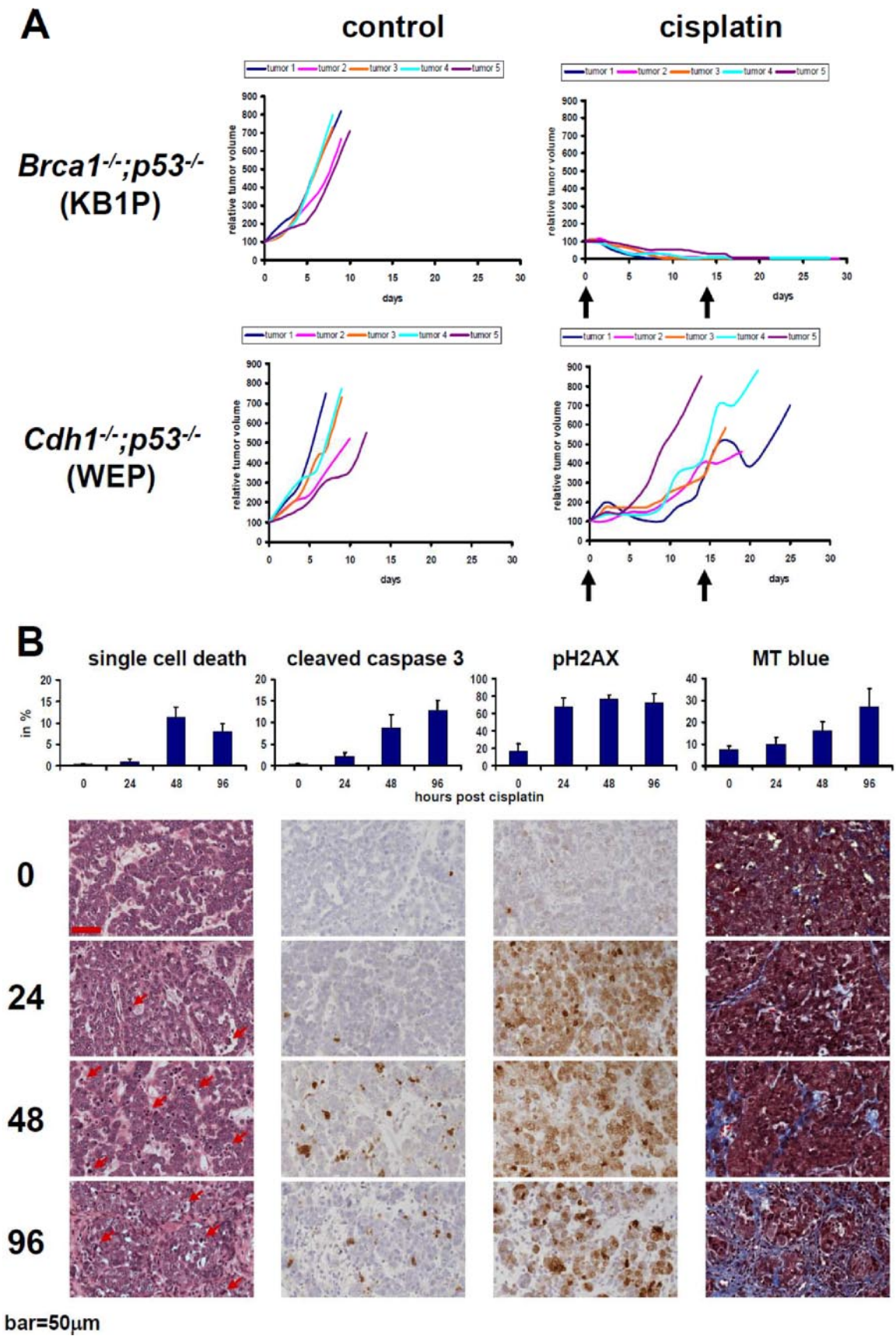
A
control
cisplatin
Brca1-/-;p53-/-
(KB1P)
Cdh1-/-;p53-/-
(WEP)
tumor 1
tumor 2
tumor 3
tumor 4
tumor 5
relative tumor volume
days
B
single cell death
cleaved caspase 3
pH2AX
MT blue
in %
hours post cisplatin
0
24
48
96
bar=50μm

band were separated on a C18 column for subsequent MS/MS analysis.

In-gel Digestion and Nano-liquid Chromatography-Q Exactive-Mass Spectrometry

Cell lysates from the FASN knockdown and control experiments were applied to a one-dimensional SDS-polyacrylamide gel. Proteins were allowed to enter the stacking gel, and the voltage was switched off when the proteins were just in the running gel. The samples on gel were processed as a single gel band and were in-gel digested with trypsin. After vacuum centrifugation, the peptide extract was filtered through a 0.45-μm low protein-binding PVDF membrane (Millipore) to remove particles. Extracted peptides were separated on a 75-μm $\times$ 20-cm custom-packed Reprosil C18 aqua column (1.9 μm, 120 Å) in a 150-min gradient (5–32% acetonitrile + 0.5% acetic acid at 300 nl/min) using a U3000 RSLC high pressure nano-LC (Dionex). Eluting peptides were measured on line by a Q Exactive mass spectrometer (ThermoFisher Scientific) operating in data-dependent acquisition mode. Peptides were ionized using a stainless steel emitter at a potential of +2 kV (ThermoScientific). Intact peptide ions were detected at a resolution of 35,000 and fragment ions at a resolution of 17,500; the MS mass range was 350–1500 Da. AGC target settings for MS were 3E6 charges and for MS/MS 2E5 charges. Peptides were selected for higher energy C-trap dissociation fragmentation at an underfill ratio of 1% and a quadrupole isolation window of 1.5 Da, peptides were fragmented at a normalized collision energy of 30. QE raw files were searched against the International Protein Index mouse 3.68 database (56,729 entries, released December 18, 2009) using MaxQuant 1.2.2.5 (13). Data was filtered at 1% false discovery rate at both the peptide and protein levels.

Data Analysis

Protein Identification—MS/MS spectra were searched against the mouse International Protein Index database 3.31 (56,555 entries, released August 17, 2007) using Sequest (version 27, revision 12), which is part of the BioWorks 3.3 data analysis package (Thermo Fisher, San Jose, CA). MS/MS spectra were searched with a maximum allowed deviation of 10 ppm for the precursor mass and 1 atomic mass unit for fragment masses. Methionine oxidation and cysteine carboxamidomethylation were allowed modifications; two missed cleavages were allowed, and the minimum number of tryptic termini was one. After database searching the DTA and OUT, files were imported into Scaffold version 1.07 (Proteome software, Portland, OR). Scaffold was used to organize the gel band data and to validate peptide identifications using the Peptide Prophet algorithm (14, 15). Only identifications with a probability >95% were retained. Subsequently, the Protein Prophet algorithm was applied, and protein identifications with a probability of >99% with two peptides or more were retained. The false discovery rate for the detected proteins using this workflow is on average around 0.5%, and it was not calculated again (16). For each protein identified, the total number of MS/MS spectra detected for each protein identified (spectral counts) was exported to Excel 2003 (Microsoft, Redmond, WA).

Spectral Count Normalization and Statistics—Normalization was performed as described previously (12, 17). A one-sided paired β-binomial test (18) was applied to find proteins that showed statistically significant differences in spectral count numbers between the untreated control tumors and the cisplatin-treated tumors, and it was applied both to the BRCA1-deficient and -proficient model. Statistical testing between the two differently treated tumor models was performed using a unpaired two-sided β-binomial test (17). Proteins with a p value of less than 0.05 were designated as being significant. Hierarchical clustering was carried out using R statistical software. For protein clustering, the abundances were normalized to zero means and unit variance for each individual protein. Subsequently, the Euclidean distance measure was used. For sample clustering, a divergence measure between two Poisson distributions was used, preventing highly abundant proteins from dominating others in contribution to the total sample difference, as described by Albrethsen *et al.* (16). The Ward linkage was used. For analysis of reproducibility, we calculated the average coefficient of variation of the spectral counts from overlapping proteins of each set of three biological replicates.

Data Mining for Functional Analyses—For STRING (Search Tool for the Retrieval of Interacting Genes/Proteins) pathway analysis (version 9.0) (19), International Protein Index identifiers were mapped to human gene symbols, after which networks were generated and downloaded. Graphical rich networks with color intensities indicating protein fold changes were made using the Cytoscape software (20) after which groups of well connected proteins were identified (21). Gene ontology analysis was performed using the BiNGO (Biological Networks Gene Ontology, Ghent, Belgium) software (22) on the top three most significant groups of well connected proteins identified by Cluster ONE (Clustering with Overlapping Neighborhood Expansion, Egham, UK).

RESULTS

BRCA1-proficient/CDH1-deficient Mammary Tumors Respond Poorly to Cisplatin—We have previously shown that BRCA1-deficient mammary tumors, which contain large intragenic deletions of the *Brca1* and *p53* genes, are highly sensitive to the maximum tolerable dose of cisplatin (3). When we treated CDH1-deficient tumors, however, we found that these hardly responded to the same regimen (Fig. 1*A*). This difference in cisplatin response between the models is not unexpected, because CDH1-deficient tumors are still capable of repairing cisplatin-induced DNA damage by homologous recombination (HR), in contrast to BRCA1-deficient tumors. In line with this, we previously observed that the CDH1-deficient tumors do not respond to treatment with the PARP inhibitor olaparib, which targets HR deficiency (23). These contrary drug responses therefore provide an opportunity to investigate differential treatment-induced protein expression in two mouse models, which carry mammary tumors that resemble specific breast cancer subtypes.

To measure proteins of viable tumor cells after treatment, we aimed at a time point when sufficient DNA damage was induced but when most drug-sensitive tumor cells had not yet entered apoptosis. Moreover, the percentage of stromal cells that eventually replace viable tumor tissue should be small. As presented in Fig. 1*B,* we found that 24 h after cisplatin ad-

FIG. 1. **Responses of *Brca1*$^{-/-}$;*p53*$^{-/-}$ (KB1P) or *Cdh1*$^{-/-}$;*p53*$^{-/-}$ (WEP) mammary tumors to cisplatin.** *A,* five individual KB1P or WEP tumors were transplanted orthotopically into syngeneic mice. Once tumors reached a volume of 200 mm^3, they were left untreated or treated with the maximum tolerable dose of cisplatin (6 mpk i.v. on days 0 and 14). *B,* analyses of drug-sensitive KB1P tumors using H&E staining (*arrows* indicate examples of cells with morphological characteristics of single cell death such as fragmented or pyknotic nuclei and hypereosinophilic cytoplasm), cleaved caspase 3, pH2AX, and Masson's trichrome stain (*MT*). *Bar,* 50 μm.

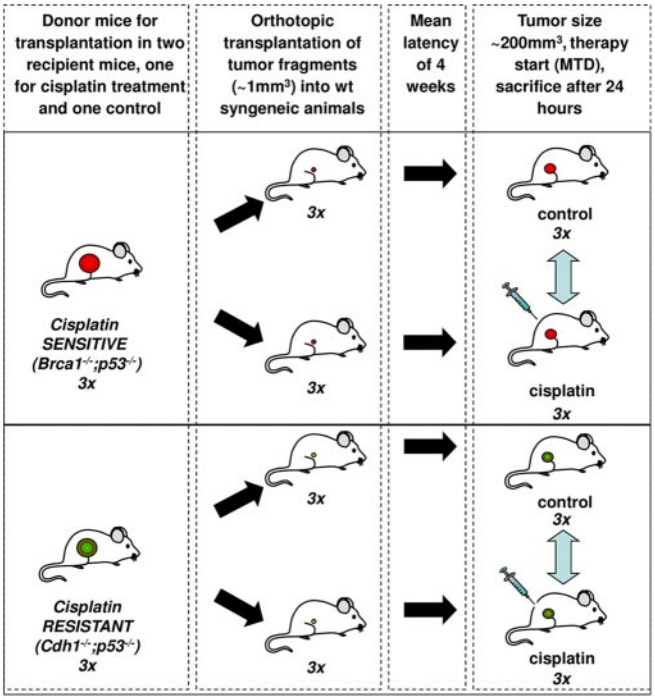

FIG. 2. **Experimental setup for the high throughput proteomics experiment using KB1P or WEP mouse models with and without cisplatin treatment.**

ministration most BRCA1-deficient tumor cells showed DNA damage foci (pH2AX), but only a few tumor cells showed morphological signs of cell death (*e.g.* pyknosis, nuclear fragmentation, or hypereosinophilic cytoplasm) or activation of caspase 3. In contrast, 48 or 96 h after treatment, the number of dying BRCA1-deficient tumor cells increased and was replaced by reactive stroma. In cisplatin-resistant (*Cdh1*$^{-/-}$;*p53*$^{-/-}$) tumors, the number of apoptotic or necrotic tumor cells was also low after 24 h of treatment as expected by the poor response (data not shown). Hence, the 24-h time point is appropriate to investigate differential induction of protein expression in cisplatin-sensitive *versus* cisplatin-resistant tumors.

Proteome Differences between Cisplatin-sensitive and -resistant Mouse Mammary Tumors Shortly after Cisplatin Treatment—To identify early response biomarkers, we used three individual cisplatin-sensitive tumors (*Brca1*$^{-/-}$;*p53*$^{-/-}$) and three cisplatin-resistant tumors (*Cdh1*$^{-/-}$;*p53*$^{-/-}$) that were either treated with cisplatin or left untreated (see Fig. 2 for experimental setup). Comparative proteomics based on SDS-PAGE (see supplemental Fig. 1*A* for gel images) in combination with nanoLC-MS/MS identified a total of 3486 proteins in the 12 mammary tumor samples using stringent protein identification criteria (only protein identifications with a probability of >99% identified with at least two peptides of >95% in one of the samples were retained). The whole dataset of identified proteins is provided in supplemental Tables 1, and supplemental Table 2 contains the peptide identifications. The number of identified proteins in each biological group was comparable and ranged from 3104 to 3206 with good reproducibility of protein identification in the four groups: 66–75% of the proteins were identified in all three biological replicates (for Venn diagrams see supplemental Fig. 1*B*).

Unsupervised cluster analysis using all 3486 proteins (supplemental Fig. 2) showed that CDH1-deficient tumors were clearly separated from the BRCA1-deficient ones. Within these groups, however, treated tumors were not separated from untreated controls. Instead, tumors derived from the same donor tumor clustered together. This result demonstrates that proteome differences between the three different tumors are larger then those induced by short term cisplatin treatment. This is consistent with previous gene expression analyses of matched tumor samples before and after acquiring drug resistance (3). Statistical analysis (18) of the cisplatin-treated *versus* -untreated samples in the sensitive model identified 167 differentially expressed proteins ($p < 0.05$). Of these, 105 were up-regulated and 62 were down-regulated (see supplemental Table 1). In the cisplatin-resistant model, we found 98 proteins differentially expressed between the control tumor and the cisplatin-treated tumor, with 68 up- and 30 down-regulated. The supplemental Table 3 contains the combined lists of the 254 proteins regulated after cisplatin treatment in the sensitive and resistant models. Importantly, supervised cluster analysis using subsets of the significantly regulated proteins that showed highly divergent properties in the two models (Fig. 3 and see below) clearly showed that the treatment and control groups are in different sub-clusters of the branches containing each model (Fig. 5 and supplemental Fig. 2, *B* and *C*), thereby underscoring the potential of a proteomics readout for assessing drug response. For a study overview that includes the different comparisons, analyses, and marker selections, see Fig. 3 and below.

Protein Interactions in Cisplatin-sensitive BRCA1-deficient Mammary Mouse Tumors after Cisplatin Treatment—To visualize interactions of the differentially expressed proteins in the sensitive BRCA1-deficient tumors before and after cisplatin treatment, we employed the STRING protein network analysis tool (19) together with graphic-rich graphs generated in Cytoscape (20). Network analysis using the Cluster ONE software (21) and BiNGO analysis (22) was used to associate subsets of proteins with biological information. To this end, we annotated the three most significant groups of well connected proteins (with a p value < 0.05 generated by Cluster ONE). Within the network of the 105 up-regulated proteins by cisplatin, Fig. 4*A* shows significant groups of highly connected nodes that were identified. The largest group of well connected proteins, containing 25 members, was associated with GO terms involving chromosome segregation during mitosis (*e.g.* "M-phase" and "chromosome segregation") and "DNA metabolic process/deoxyribonucleotide metabolic process". See Fig. 4*E* and supplemental Table 4A for BiNGO analysis results on the regulated proteins and the significant

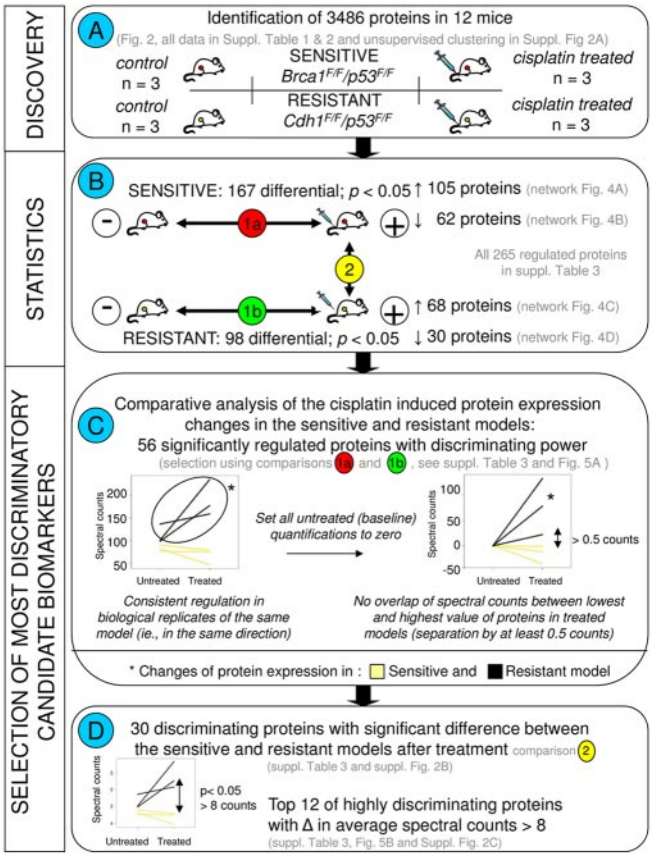

FIG. 3. **Flow chart depicting the different comparisons and criteria for selection of the most discriminatory biomarkers.** *A*, describes the discovery experiment including four groups consisting of cisplatin-sensitive and -resistant models with the control and cisplatin treatment groups for each model, with three animals in each group. *B*, displays the statistical comparisons. All statistical analyses were performed using R as described previously (17, 18). To select the most discriminatory markers , we applied quantitative filtering in Excel. To this end, protein spectral count data of the 3486 proteins were exported from Scaffold to Excel. Paired statistical testing (18) in R identifies differentially expressed proteins between the treated and untreated tumors in each tumor type separately (comparisons *1a* and *1b*). *C*, shows the criteria to select for proteins with divergent regulation in the sensitive and resistant model. To this end, base-line transformation was applied to each protein. Furthermore, only proteins were retained that displayed a minimum separation of 0.5 counts between the lowest and the highest value in the two models after cisplatin treatment. This led to a selection of 56 discriminatory candidate markers. *Left graph,* example of untransformed spectral counts for the sensitive and resistant paired sets. *Right graph,* example using the same protein, with untreated tumors brought to a base line of zero counts. *D*, further selection was made to pinpoint the most discriminatory proteins. Using β-binomial statistics (17) on the list of 56 proteins, we selected 30 proteins who were significantly different between the sensitive and resistant models after cisplatin treatment (comparison *2* in *B*). From these 30 proteins, the top 12 was selected with highly divergent regulation patterns in the two models, *i.e.* proteins displaying on average at least eight counts of separation between the average values in both models after treatment (before base-line transformation).

groups of well connected proteins. Well known examples of chromosome segregation proteins include multiple kinesins (KIF11, KIF23, and KIF4B) as well as centrosome-related proteins (INCENP, CENPE, KNTC1, and AURKB). Also, chromosome condensation proteins were up-regulated (NCAPG and NCAPH). In the GO category "nucleic acid metabolic process," we detected proteins such as TOP2A, RRM1, and DTYMK. In addition, this cluster includes DNA repair proteins such as MRE1A, poly(ADP-ribose) polymerase 1 (PARP1), FEN1, and LIG1. The second group contained eight proteins (Fig. 4*A*) involved in a "multiorganism process" and "response to biotic stimulus." The third group consisted of five members (Fig. 4*A*) that are mainly involved in RNA splicing with GO terms like "RNA splicing" and "RNA metabolic process" (Fig. 4*E* and supplemental Table 4A). FXR1, an RNA-binding protein that is not a member of this group, was also up-regulated. Other proteins of interest but not included in the top three groups are CHD4, a modulator of homologous repair (24), the DNA-associated protein NCOR2, a chromatin remodeler, and the histone-binding protein NASP.

When visualizing the down-regulated proteins in BRCA1-deficient tumors after cisplatin treatment as a protein-protein interaction network using the STRING tool (see Fig. 4*B*), we identified two large groups of well connected proteins of 14 and 9 proteins related to inflammatory response as indicated by GO terms like "response to wounding" and "inflammatory response" (and Fig. 4*E* and supplemental Table 4B). The main difference between the two groups is that proteins in group 1 are mainly localized in the extracellular space, whereas the smaller group 2 contains predominantly intracellular proteins that are also implicated in regulation of vesicle-mediated transport, response to oxidative stress, and anti-apoptosis. The majority of proteins in the third group are associated with "carbohydrate metabolic process" with ITIH1, ITIH2, and ITIH3 involved in the transport of the carbohydrate polymer hyaluronan. Other proteins outside this group (*e.g.* PC, MAGT1, and HK1) are also implicated in carbohydrate metabolism. A total of 34 proteins within the 62 down-regulated proteins fell within the GO term called "metabolic process" suggesting major down-regulation of metabolic proteins.

In conclusion, the proteomics and gene ontology data of early cisplatin response show that DNA segregation/metabolism/repair and inflammatory response are the major biological processes altered in the sensitive *Brca1*$^{-/-}$;*p53*$^{-/-}$ tumors after cisplatin treatment.

Protein Interactions in Cisplatin-resistant Mammary Mouse Tumors after Cisplatin Treatment—Protein network analysis in the cisplatin-resistant model using the 68 up-regulated proteins after cisplatin treatment revealed two main groups of well connected proteins with functions involved in fatty acid synthesis and chromosome/centrosome regulation as identified in Cluster ONE/BiNGO analysis (see Fig. 4*C*). The first sub-network is associated with fatty acid synthesis, as indicated by the GO terms "fatty acid metabolic process" and

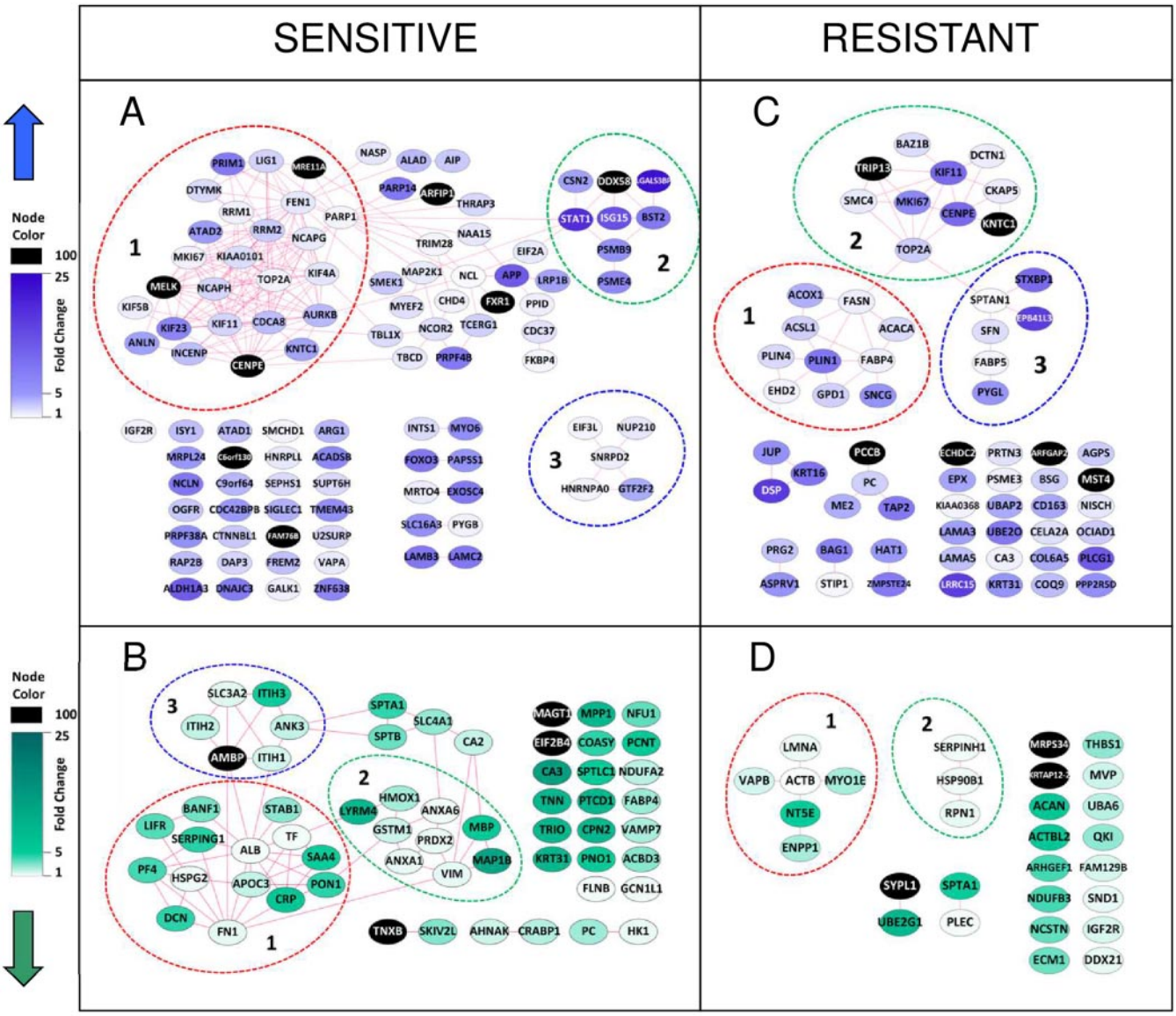

E

Regulation after Cisplatin Tx	# proteins	Cluster	# proteins/cluster	Gene Ontolgy (GO) term	# proteins	Cluster	# proteins	Gene Ontolgy (GO) term
				Sensitive				**Resistant**
↑	105 (panel 4 A)	1	25	Chromosome segregation DNA/deoxyribonucleotide metabolic process	68 (panel 4 C)	1	10	Fatty acid metabolic process Lipid metabolic process
		2	8	Multi-organism process Response to biotic stimulus		2	10	M phase of mitotic cell cycle
		3	5	RNA splicing RNA metabolic process		3	6	Regulation of biological quality
↓	62 (panel 4 B)	1	14	Response to wounding (extracellular) Acute inflammatory response (extracellular)	30 (panel 4 D)	1	6	Nucleotide catabolic process ER-nucleus signaling pathway
		2	9	Response to wounding (intracellular) Inflammatory response (intracellular)		2	3	Ubiquitin-dependent protein catabolic process Protein catabolic process
		3	6	Carbohydrate metabolic process				

"lipid metabolic process" (see Fig. 4*E* and supplemental Table 4C). Some of these proteins are known to be involved mainly in *de novo* fatty acid synthesis and/or fatty acid degradation (*e.g.* FASN, ACACA, ACOX1, and ACSL1), whereas others function in mechanisms related to lipid storage or transport (*e.g.* FABP4 and PLIN1). In addition, synuclein γ, a known interactor of FABP4 (25) with a hypothesized lipid binding domain, was up-regulated.

The second group contained mostly chromosome/centromere proteins that function during cell division (*e.g.* GO term "M phase of mitotic cell cycle"). Members include TRIP13, involved in chromosome recombination and chromosome structure development during meiosis, and also KNTC1, an essential component of the mitotic checkpoint. The third group is involved in "regulation of biological quality" with a diverse set of sub-functions within this GO term (supplemental Table 4C). STXBP1 functions as a vesicle-membrane regulating protein, whereas SPTAN1 is responsible for cytoskeletal movement near the membrane, but it is also implicated in DNA repair and the cell cycle. PYGL, an enzyme functioning within the carbohydrate metabolism, was also present in this group. Moreover, outside the three main clusters, a number of other proteins are involved in metabolism, including PC, CAR3, ME2, and PCCB.

The protein network of the down-regulated proteins (see Fig. 4*D*) contained two groups of well connected proteins as follows: the first and main group is associated with the GO terms "nucleotide catabolic process" (NT5E and ENPP1) and "ER-nucleus signaling pathway" (VAPB and LMNA, also see Fig. 4*E* and supplemental Table 4D), and the second smaller group includes proteins associated mostly to "ubiquitin-dependent protein catabolic process" and "protein catabolic process" (HSP90B1 and RPN1). Overall, seven out of the 30 proteins in Fig. 4*D* are involved in "cellular catabolic process" and are included, for example, in UBA6 and UBE2G1, two enzymes functioning as ubiquitination proteins.

In summary, fatty acid metabolism and the M phase of the cell cycle are the major processes associated with the up-regulated proteins after short term cisplatin treatment in resistant tumors, whereas several proteins involved in catabolic processes are down-regulated.

Selection of FASN for Functional Follow Up—To identify cisplatin response markers showing the most diverging pattern between sensitive and resistant models, we selected proteins with optimal separating properties by applying a number of filtering criteria on the differential proteins identified using the paired statistics (Fig. 3 and supplemental Table 3 for all relevant criteria used for inclusion). First, we reasoned that the more robust markers are those proteins whose regulation is consistent in all biological replicates (*i.e.* in the same direction) and that have an average fold change of minimally 1.5. Next, we selected proteins with divergent regulation in the cisplatin-sensitive and -resistant models (Fig. 3*C*). To this end, we brought all protein quantifications of the untreated tumors to a base line of zero counts, whereby the protein quantifications of the matching treated tumors were adjusted in the same way for each protein separately. After this base-line transformation, we selected proteins whose normalized spectral counts in the treated tumors did not overlap between the sensitive and the resistant models. See Fig. 3*C* for a graphical example. This resulted in 56 top discriminatory candidates that are described in Table I (also see supplemental Table 3 for detailed quantitative information). These top 56 discriminatory proteins showed an optimal clustering pattern that could separate the four groups in a supervised clustering (Fig. 5*A*). For a further selection of proteins with optimal separation power, we selected proteins that were significantly differential between the two cisplatin-treated groups ($p < 0.05$, using the unpaired β-binomial test (17)), yielding 30 proteins (Fig. 3*D*). Of these, 12 proteins displayed strong opposite regulations as revealed by applying a cutoff of eight spectral counts between the averaged spectral counts of the two treated groups (Fig. 3*D*) (both criteria implemented before base-line transformation). Both top lists also displayed optimal clustering patterns. See supplemental Fig. 2, *B* and *C*, for the supervised hierarchical clustering results of the 30 and 12 most discriminatory proteins, respectively. Fig. 5*B* displays expression profiles for the 12 proteins. We chose FASN for targeted follow up because it showed the largest quantitative difference (123 spectral counts) between the two models after treatment and because of its involvement in one of the major discriminatory pathways, namely fatty acid metabolism.

FASN Knockdown Sensitizes Resistant Cells for Cisplatin Treatment—In a proof-of-concept experiment, we determined whether inhibition of the fatty acid metabolism sensitizes *Cdh1*$^{-/-}$;*p53*$^{-/-}$ tumor cells to cisplatin. For this purpose, we transduced KEP11 cells with two *Fasn*-targeting shRNA constructs. These resulted in target inhibition of about 60% for mRNA and protein expression levels (Fig. 6, *A* and *B*). There was no alteration of cell proliferation for the transduced cells (Fig. 6*C*). When we tested the cells expressing these hairpins for cisplatin sensitivity, we found that cells with a lower *Fasn*

FIG. 4. **Protein-protein networks of the regulated proteins selected using a paired statistical analysis between treated and untreated conditions.** The networks were generated using default settings in String (and visualized using Cytoscape. *Dashed lines* indicate the top three most significant clusters identified by Cluster ONE analysis. *Nodes* represent proteins, and the edges represent interactions that include direct (physical) and indirect (functional) associations. See Szklarczyk *et al.* (19) for more details on edge generation. *A,* up-regulated proteins in the cisplatin-sensitive tumors. *B,* down-regulated proteins in the cisplatin-sensitive tumors. *C,* up-regulated proteins in the cisplatin-resistant tumors. *D,* down-regulated proteins in the cisplatin-resistant tumors. *E,* representative GO terms identified by BiNGO analysis for the top three clusters within the regulated proteins.

TABLE I

Top discrimination proteins between BRCA1-deficient and -proficient mammary tumors after short term cisplatin treatment

NA means not applicable.

Description	International protein index	Gene ontology	Human gene names	Significant regulation in sensitive model[a]	Fold change in sensitive model[a]	*p* value in sensitive tumors[a]	Significant regulation in resistant model[a]	Fold change in resistant model[a]	*p* value in resistant tumors[a]	Top 30 proteins[b]	Top 12 proteins[c]
Fatty-acid synthase	IPI00113223	Lipid metabolic process	*FASN*		−1.3	0.0697	↑	1.7	0.0173	x	x
Ki_r-67 protein	IPI00124959	M phase	*MKI67*	↑	1.5	0.0118	↑	7.1	0.0062	x	x
Carbonic anhydrase 3	IPI00221890	Small molecule metabolic process	*CA3*	↓	−13.9	0.0000	↑	1.6	0.0089	x	x
Fatty acid-binding protein, adipocyte	IPI00116705	Lipid metabolic process	*FABP4*	↓	−2.6	0.0099	↑	1.6	0.0066	x	x
Chromodomain-helicase-DNA-binding protein 4	IPI00396802	Chromosome organization	*CHD4*	↑	1.6	0.0221		−1.0	0.4882	x	x
Nuclear pore membrane glycoprotein 210 precursor	IPI00342158	Establishment of protein localization	*NUP21*	↑	1.9	0.0110		−2.0	0.2815	x	x
Kinesin-like protein KIF11	IPI00130218	Mitotic spindle organization	*KIF11*	↑	2.6	0.0106	↑	11.1	0.0281	x	x
EH domain-containing protein-2 homolog	IPI00402968	Organelle organization	*EHD2*		−2.3	0.0996	↑	1.5	0.0470	x	x
Glutathione *S*-transferase Mu 1	IPI00230212	Metabolic process	*GSTM1*	↓	−1.8	0.0252		1.2	0.2058	x	x
Pyruvate carboxylase, full insert sequence	IPI00114710	Lipid metabolic process	*PC*	↓	−2.5	0.0144	↑	2.8	0.0261	x	x
Perilipin	IPI00223783	Lipid metabolic process	*PLIN1*		−1.1	0.3851	↓	−1.6	0.0334	x	x
Condensation protein G isoform 1	IPI00122202	M phase	*NCAPG*	↑	1.9	0.0171		1.4	0.2403	x	x
Major vault protein	IPI00111258	mRNA transport	*MVP*		2.0	0.2809	↓	−3.3	0.0378	x	
Small nuclear ribonucleoprotein Sm D2	IPI00119220	Nucleic acid metabolic process	*SNRPD*	↑	1.7	0.0320		−1.1	0.4066	x	
γ-Synuclein	IPI00271440	Regulation of neurotransmitter secretion	*SNCG*		−3.8	0.1126	↑	5.7	0.0045	x	
Thymidylate kinase, full insert sequence	IPI00831272	Deoxyribonucleotide biosynthetic process	*DTYMK*	↑	2.4	0.0189		−1.3	0.2717	x	
Galactokinase 1	IPI00265025	Monosaccharide metabolic process	*GALK1*	↑	1.6	0.0425		−1.2	0.2653	x	
Isoform 1 of nuclear autoantigenic sperm protein	IPI00130959	Chromosome organization	*NASP*	↑	2.0	0.0242		1.4	0.2464	x	
Kinesin family member 23	IPI00407864	Mitotic spindle organization	*KIF23*	↑	7.7	0.0030		1.7	0.3034	x	
Flap structure-specific endonuclease 1, full insert	IPI00410836	Nucleic acid metabolic process	*FEN1*	↑	1.9	0.0350		2.0	0.0937	x	
Tubulin-specific chaperone D	IPI00461857	Macromolecule metabolic process	*TBCD*	↑	1.9	0.0447		−1.5	0.1893	x	
Actin-binding protein anillin	IPI00172197	Nuclear division	*ANLN*	↑	4.7	0.0078		7.0	0.0597	x	

TABLE I—*continued*

Description	International protein index	Gene ontology	Human gene names	Significant regulation in sensitive model[a]	Fold change in sensitive model[a]	*p* value in sensitive tumors[a]	Significant regulation in resistant model[a]	Fold change in resistant model[a]	*p* value in resistant tumors[a]	Top 30 proteins[b]	Top 12 proteins[c]
Ribonucleoside-diphosphate reductase M2 subunit	IPI00112645	Deoxyribonucleotide biosynthetic process	*RRM2*	↑	3.0	0.0249		2.0	0.2784	x	
Isoform 1 of Mitochondrial 28 S ribosomal protein S29	IPI00275050	Cellular component organization	*DAP3*	↑	2.6	0.0332		−1.0	0.4984	x	
Isoform 1 of Borealin	IPI00621765	M phase	*CDCA8*	↑	3.5	0.0420		1.0	1.0000	x	
Pre-mRNA-splicing factor ISY1 homolog	IPI00469994	Nucleic acid metabolic process	*ISY1*	↑	3.5	0.0431		−1.7	0.3100	x	
39S ribosomal protein L24, mitochondrial precursor	IPI00162769	Macromolecule biosynthetic process	*MRPL2*	↑	5.0	0.0435		1.0	1.0000	x	
Uncharacterized protein C6orf130 homolog	IPI00154005	Purine nucleoside binding	*C6orf1*	↑	100.0	0.0106		1.0	1.0000	x	
Isoform 1 of protein FAM76B	IPI00330763	NA	*FAM76*	↑	100.0	0.0108		1.0	1.0000	x	
Maternal embryonic leucine zipper kinase	IPI00323045	Cellular macromolecule metabolic process	*MELK*	↑	100.0	0.0108		1.0	1.0000	x	
Ligase I, DNA, ATP-dependent	IPI00473314	Nucleic acid metabolic process	*LIG1*	↑	2.7	0.0097		1.5	0.1850		
Cation-independent mannose 6-phosphate receptor	IPI00308971	Positive regulation of apoptosis	*IGF2R*	↑	1.5	0.0497	↓	−1.6	0.0351		
Glutathione *S*-transferase, θ3	IPI00116236	Glutathione metabolic process	*Gstt3*	↑	2.9	0.0358		1.0	0.4967		
Hsp90 co-chaperone Cdc37	IPI00117087	M phase	*CDC37*	↑	2.1	0.0200		1.0	0.4925		
Thyroid hormone receptor-associated protein 3	IPI00556768	Nucleic acid metabolic process	*THRAP*	↑	2.5	0.0143		1.0	0.4933		
Isoform E of Fragile × mental retardation syndrome-related protein 1	IPI00122521	Regulation of translation	*FXR1*	↑	100.0	0.0019		−1.3	0.2467		
Isoform 2 of U2-associated protein SR140	IPI00467507	RNA processing	*U2SUR*	↑	2.4	0.0401		1.2	0.3749		
Aggrecan core protein precursor	IPI00119035	Proteolysis	*Acan*		1.0	1.0000	↓	−6.1	0.0054		
mRNA turnover protein 4 homolog	IPI00132578	Ribosome biogenesis	*MRTO4*	↑	1.7	0.0457		1.2	0.3036		
Isoform 7 of protein quaking	IPI00130483	mRNA transport	*QKI*		−1.0	0.4981	↑	9.4	0.0004		
Monocarboxylate transporter 4	IPI00118910	Monocarboxylic acid transport	*SLC16*	↑	6.0	0.0272		−1.0	0.4990		
Carbonic anhydrase 2	IPI00121534	Metabolic process	*CA2*	↓	−1.9	0.0353		1.1	0.4305		
Myosin IE	IPI00330649	Vasculogenesis	*MYO1E*		1.3	0.2303	↓	−1.7	0.0495		
Niban-like protein	IPI00330695	Negative regulation of apoptotic process	*FAM12*		−1.4	0.3426	↓	−1.8	0.0208		
Vesicle-associated membrane protein-associated protein	IPI00135655	Nucleotide catabolic process	*VAPB*		3.0	0.1509	↓	−6.0	0.0261		

TABLE I—*continued*

Description	International protein index	Gene ontology	Human gene names	Significant regulation in sensitive model[a]	Fold change in sensitive model[a]	*p* value in sensitive tumors[a]	Significant regulation in resistant model[a]	Fold change in resistant model[a]	*p* value in resistant tumors[a]	Top 30 proteins[b]	Top 12 proteins[c]
Isoform 1 of double strand break repair protein MRE11A	IPI00118853	Nucleic acid metabolic process	*MRE11*	↑	100.0	0.0106		−1.7	0.3082		
Vesicle-associated membrane protein-associated protein	IPI00125267	Cellular membrane fusion	*VAPA*	↑	1.9	0.0333		−1.3	0.1713		
Isoform 2 of acetyl-CoA carboxylase 1	IPI00848443	Lipid metabolic process	*ACACA*		1.5	0.2119	↓	−2.7	0.0342		
ADP-ribosylation factor interacting protein 1	IPI00466057	Establishment of localization in cell	*ARFIP1*	↑	100.0	0.0057		−2.0	0.1596		
Actin, cytoplasmic type 5 homolog	IPI00221528	Nucleotide and ATP binding	*ACTBL*		1.1	0.2369	↑	2.4	0.0200		
Isoform 1 of translation initiation factor eIF-2B subunit	IPI00124879	Metabolic process	*EIF2B4*	↓	−100.0	0.0116		3.0	0.1514		
Pno1 RNA-binding protein PNO1	IPI00131909	RNA binding	*PNO1*	↓	−5.0	0.0444		1.0	0.4991		
Isoform Long of Extracellular matrix protein 1 precursor	IPI00122272	System development	*ECM1*		−1.3	0.2637	↓	−2.4	0.0106		
Itih1 protein	IPI00322867	Metabolic process	*ITIH1*	↓	−1.7	0.0130		1.1	0.2890		
Ubiquitin-activating enzyme E1-like protein 2	IPI00226815	Proteolysis involved in cellular protein catabolic process	*UBA6*		2.8	0.0556	↓	−2.1	0.0358		
Golgi resident protein GCP60	IPI00129907	Metabolic process	*ACBD3*	↓	−2.9	0.0442		7.0	0.0597		

[a] The fold change and one-sided *p* value were calculated between protein levels in control and treated tumors.
[b] Top proteins with an average eight spectral count difference between treated tumors are given.
[c] Proteins with significant ($p > 0.05$, two-sided) difference between treated tumors are shown.

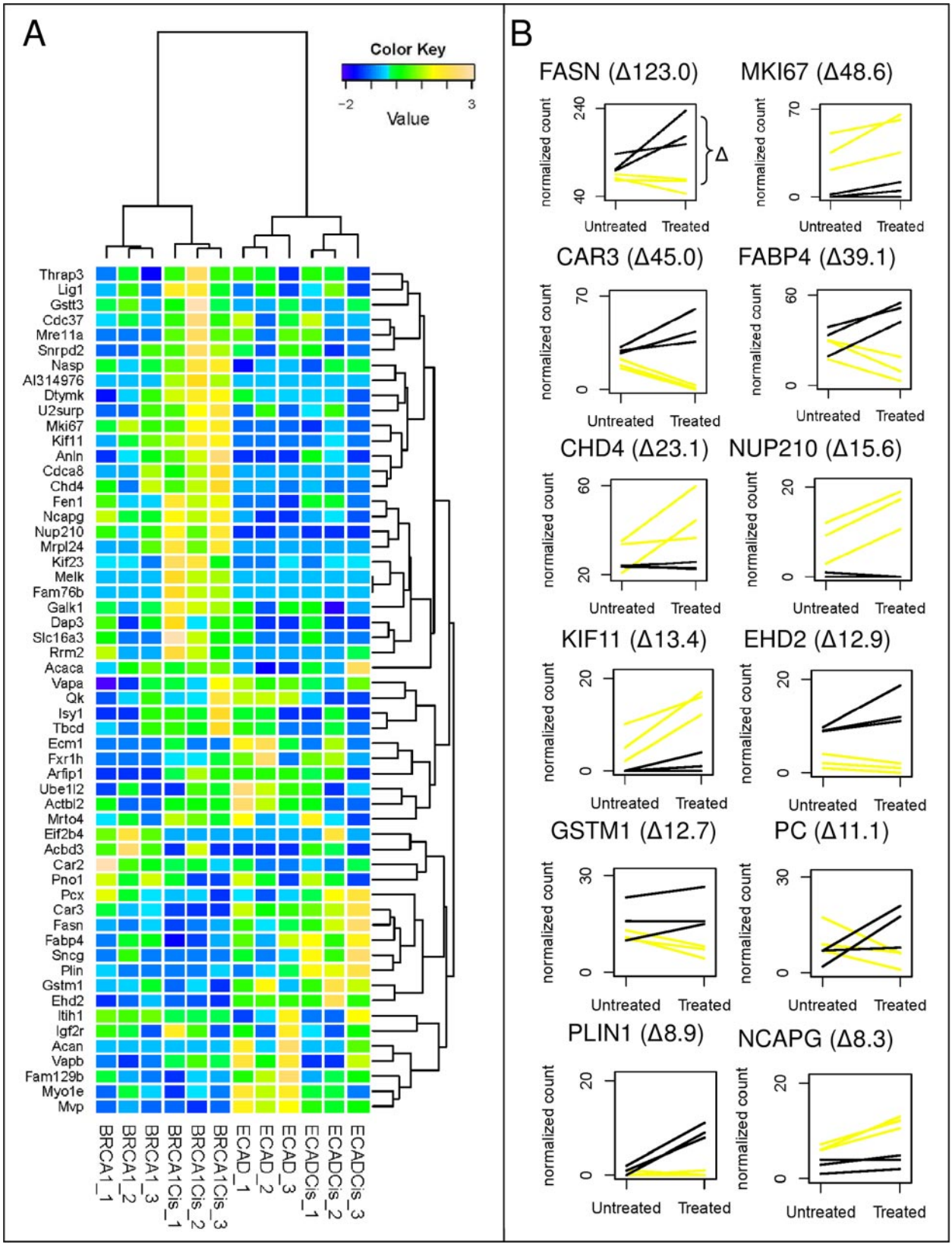
A
Color Key
−2
3
Value
Thrap3
Lig1
Gstt3
Cdc37
Mre11a
Snrpd2
Nasp
AI314976
Dtymk
U2surp
Mki67
Kif11
Anln
Cdca8
Chd4
Fen1
Ncapg
Nup210
Mrpl24
Kif23
Melk
Fam76b
Galk1
Dap3
Slc16a3
Rrm2
Acaca
Vapa
Qk
Isy1
Tbcd
Ecm1
Fxr1h
Arfip1
Ube1l2
Actbl2
Mrto4
Eif2b4
Acbd3
Car2
Pno1
Pcx
Car3
Fasn
Fabp4
Sncg
Plin
Gstm1
Ehd2
Itih1
Igf2r
Acan
Vapb
Fam129b
Myo1e
Mvp
BRCA1_1
BRCA1_2
BRCA1_3
BRCA1Cis_1
BRCA1Cis_2
BRCA1Cis_3
ECAD_1
ECAD_2
ECAD_3
ECADCis_1
ECADCis_2
ECADCis_3
B
FASN (Δ123.0)
MKI67 (Δ48.6)
CAR3 (Δ45.0)
FABP4 (Δ39.1)
CHD4 (Δ23.1)
NUP210 (Δ15.6)
KIF11 (Δ13.4)
EHD2 (Δ12.9)
GSTM1 (Δ12.7)
PC (Δ11.1)
PLIN1 (Δ8.9)
NCAPG (Δ8.3)
normalized count
Untreated
Treated
Δ

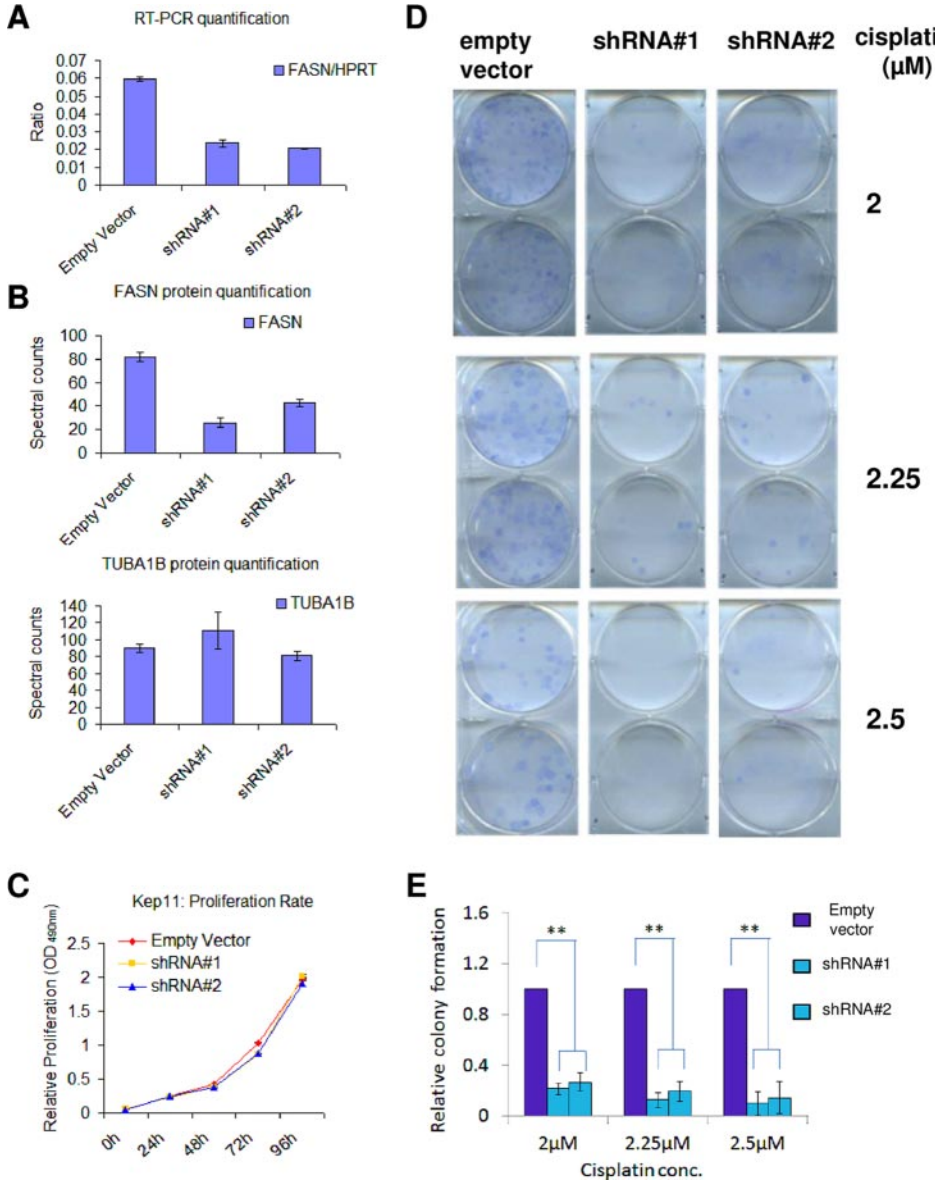

FIG. 6. ***Fasn* knockdown and clonogenic survival after cisplatin treatment in *Cdh1*$^{-/-}$;*p53*$^{-/-}$ (KEP11) cells.** *A,* knockdown efficacy of two shRNA hairpins targeting *Fasn* and an empty vector as determined by quantitative RT-PCR. *Hprt* gene expression was used as reference. All experiments were performed in triplicate, and the *error bars* indicate S.D. (also for *B* and *C*). *B,* knockdown efficacy of the same two shRNA hairpins targeting and empty vector at the protein level as determined by mass spectrometry. TUBA1B expression is shown as a reference. *C,* proliferation rate of the cell lines transduced with the two *Fasn*-targeting shRNAs and empty vector. *D,* clonogenic survival of the cell lines transduced with the two *Fasn*-targeting shRNAs and empty vector after cisplatin treatment. Six, 8, or 9 days after treatment with 2, 2.25, or 2.5 μM cisplatin, respectively, the surviving colonies were stained. This experiment was carried out in triplicate, and a representative result is shown. *E,* quantification of *D*. Average colony numbers of cells with the *Fasn*-targeting shRNAs are presented relative to the number of colonies of the control cells. The *error bars* indicate S.D., and ** indicates a $p < 0.001$ (Student's *t* test).

gene expression were more sensitive to cisplatin (Fig. 6*D*). We obtained the same result when we transduced another *Cdh1*$^{-/-}$;*p53*$^{-/-}$ cell line (called KEP23) with the indicated control or sh*Fasn* constructs (data not shown). These data suggest that targeting fatty acid metabolism may be a useful therapeutic strategy to sensitize the cisplatin-resistant tumors

FIG. 5. *A,* hierarchical cluster analysis of the top 56 discriminatory proteins, showing complete separation of all four control and treatment conditions of the cisplatin-sensitive (KB1P) and -resistant (WEP) tumors. *B,* expression profiles using spectral counting of the 12 significant proteins with at least eight spectral count differences between the two treated tumor types. Expression profiles were constructed using normalized spectral counts. *Lines* connect paired samples before and after treatment. *Yellow lines* represent the three sensitive tumors before and after treatment, and *black lines* represent the resistant tumors.

and further emphasizes the validity of our approach for finding candidate biomarkers that are predictive of cisplatin treatment.

DISCUSSION

In this study, we generated proteome signatures after a short pulse of cisplatin treatment using two mouse models for specific breast cancer subtypes that display a marked difference in drug response. We report a comprehensive dataset of about 3400 proteins with 167 and 98 differentially expressed in the sensitive and resistant model, respectively. To our knowledge, this study provides the first and largest proteomic screen to date to identify cisplatin-responsive candidate markers shortly after treatment. Most notably, we identified highly discriminatory protein subsets of 56, 30, and 12 proteins that showed diverging patterns in the two models and could separate all four conditions using hierarchical clustering (see flowchart in Fig. 3 for selection of different discriminatory subsets).

To predict chemotherapy response, the additional use of tumor samples taken shortly after the first treatment may be advantageous over the common practice to find predictive markers only by using unchallenged tumors. This approach is encouraged by the recent finding that low scores of RAD51 foci, assessed 24 h after the first chemotherapy cycle, help to find patients with breast cancers that are defective in DNA repair by HR (26). Future clinical trials will show whether the predictive value of RAD51 scores is sufficient to identify patients who may benefit from DNA repair-targeting therapy, such as PARP inhibition.

In our study we used cisplatin, because platinum drugs are frequently applied in the clinic to treat cancer patients. In particular, platinum drugs may be helpful to treat breast cancer patients with HR-defective tumors (4, 5). This is consistent with our previous finding that mammary tumors generated in our mouse model for BRCA1-deficient tumors are highly sensitive to cisplatin (3).

In these tumors, we found that up-regulated proteins after cisplatin treatment were mostly involved in DNA repair, DNA metabolism, and chromosome segregation. Of these, only three (TOP2A, KIF11, and KNTC1) were also significantly up-regulated in the cisplatin-resistant tumors. Previously, we showed major up-regulation of DNA repair proteins in drug-naive BRCA1-deficient mouse tumors (12). Consistent with the important role that BRCA1 plays in the DNA damage response (27), we illustrate that DNA damage repair is further challenged in response to treatment with the DNA-damaging agent cisplatin. In the absence of a proper homology-directed DNA repair, more pressure appears to be put on other DNA repair mechanisms. This is indicated by the increased levels of enzymes involved in single-stranded DNA break repair such as PARP1, FEN1, and LIG1. Moreover, up-regulated MRE11A suggests that more error-prone nonhomologous end-joining may occur to repair double-stranded DNA breaks.

One of the down-regulated proteins in the BRCA1 model that is part of the top 12 proteins, GSTM1, is involved in glutathione metabolism and acts as detoxification protein. GSTM1 and other glutathione *S*-transferases have been linked with differences in cisplatin response (28).

In the cisplatin-resistant model, a remarkable finding was that fatty acid metabolism proteins were the most significant up-regulated cluster. Some of these proteins (FABP4, CA3, and PC) were also significantly down-regulated in the sensitive (BRCA1-deficient) model. This indicates a good resolving power to distinguish the two models in a short term treatment setting and suggests the potential usefulness of such markers for cisplatin resistance.

Among the top 56 discriminatory proteins, FASN and ACACA are two core proteins involved in *de novo* fatty acids synthesis, of which FASN showed the largest quantitative difference between the two models after cisplatin treatment. Proliferating cancer cells have a highly up-regulated *de novo* fatty acid synthesis to provide sufficient lipids for membrane components, β-oxidation, and lipid modification of proteins. In human breast cancer cell lines, vector-induced FASN overexpression has been shown to increase resistance to cisplatin as well as inducing overexpression of ERBB2, a receptor tyrosine kinase that induces cell proliferation (29). In CDH1-deficient cells derived from our mouse model, we do not find a change in proliferation after FASN inhibition. FASN inhibition has also been described as a sensitizer for cisplatin treatment in mice xenografted with human ovarian cancer cells (30). In fact, FASN is highly expressed across a wide range of human tumor types where its inhibition either induces apoptosis and/or synergizes with cytotoxic agents (31–38). Consistent with these data, we show that inhibition of FASN with short hairpin RNAs also sensitized our CDH1-deficient cells to cisplatin treatment. In contrast to previous FASN inhibitors that displayed off-target effects and induced weight loss, novel FASN inhibitors are currently being developed that specifically target only FASN and shown encouraging *in vitro* and *in vivo* anti-cancer activity in human breast cancer (39–41).

Another more complex functional link between fatty acids and cisplatin resistance has recently been described in xenotransplantation models. Specific unsaturated platinum-induced fatty acids secreted from circulating mesenchymal stem cells cause cisplatin resistance (42). The precise mechanism by which these platinum-induced fatty acids induce resistance still remains to be elucidated, and we are currently investigating whether there is an effect of platinum-induced fatty acids on our BRCA1-defective tumors.

In this study, we did not only identify proteins involved in *de novo* fatty acid synthesis (*e.g.* FASN and ACACA) but also in fatty acid signaling, transport, and storage. Two of our top discriminatory proteins, FABP4 and γ-synuclein, have lipid binding potential, whereas PLIN is involved in lipid droplet storage. Lipid droplet accumulation has been correlated with malignancy and chemotherapy treatment. FABP4 is thought

to bind primarily palmitic acid, although the majority of the fatty acid-binding protein family, including FABP4, has a more broader binding affinity for different fatty acid structures (43). FABP4 can activate PPARγ signaling when translocated to the nucleus. PPARγ regulates fatty acid storage and glucose metabolism. FABP4 has also been described as a PTEN interactor, whose loss has been described as an activator of cancer-specific metabolic activity. Also, PTEN loss has been shown to increase FABP4 expression. Recently, FABP4 was implicated as an important mediator for metastasis to fat-rich tissues (44), whereby FABP4 was used to transport fatty acids from the fat cell to cancer cells. Furthermore, activated AMP kinase, a known inhibitor of FASN and ACACA, two of our top discriminatory proteins, has been shown to inhibit PPARγ. AMP kinase, a major metabolic sensor, is frequently inactivated in a wide range of cancers. Recently CA3, also a major discriminatory enzyme, has been described to be functionally involved with PPARγ in adipose tissue (45). Moreover, proteins with established roles in double-stranded DNA repair (*e.g.* BRCA1 and DNA-PK) have been implemented as regulators of fatty acid metabolism (46, 47). Combined, our data point toward an intricate cooperation between metabolic and DNA repair proteins when tumors with differential BRCA1 status are treated with cisplatin.

In summary, we showed the feasibility of proteomic profiling in mouse tumor models to assess treatment outcome for cisplatin treatment. Early treatment profiling to predict therapy outcome might also be useful for less toxic treatments such as PARP inhibitors, which specifically target HR-deficient tumors. Our proteomic screen identified proteins involved in DNA repair and cancer (fatty acid) metabolism as the major discriminators between sensitive and resistant tumors shortly after cisplatin treatment. These proteins may contribute to functionally test whether tumors respond to anti-cancer therapy. Because finding markers that distinguish drug-resistant from drug-sensitive tumors before treatment starts has proven to be difficult, the analysis of protein changes shortly after initial treatment may facilitate clinical decision making and help to optimize personalized treatments.

Acknowledgment—We thank Piet Borst for critical reading of the manuscript.

* This work was supported in part by CenE/Van Lanschot (to M.W.), the VUMC-Cancer Center Amsterdam (to C.R.J., T.V.P., and Proteomics Infrastructure), CTMM BreastCare (to S.R. and J.J.), the Dutch Cancer Society project grants (to S.R. and J.J.), the Netherlands Organization for Scientific Research Vidi grant (to S.R.), and the WO Cancer Systems Biology Center grant (to J.J.).

[S] This article contains supplemental material.

§ Both authors contributed equally to this work.

** Supported by a TopTalent fellowship from the NWO.

‡‡ To whom correspondence may be addressed: Division of Molecular Biology and Centre for Biomedical Genetics, The Netherlands Cancer Institute, Plesmanlaan 121, 1066 CX Amsterdam, The Netherlands. Tel.: 31-205122082; Fax: 31-206691383; E-mail: s.rottenberg@nki.nl.

§§ To whom correspondence may be addressed: OncoProteomics Laboratory, CCA 1-60, Dept. of Medical Oncology, VUMC-Cancer Center Amsterdam, VU University Medical Center, De Boelelaan 1117, 1081 HV Amsterdam, The Netherlands. Tel.: 31-204442340; Fax: 31-204443844; E-mail: c.jimenez@vumc.nl.

REFERENCES

1. Borst, P., and Wessels, L. (2010) Do predictive signatures really predict response to cancer chemotherapy? *Cell Cycle* **9,** 4836–4840
2. Liu, X., Holstege, H., van der Gulden, H., Treur-Mulder, M., Zevenhoven, J., Velds, A., Kerkhoven, R. M., van Vliet, M. H., Wessels, L. F., Peterse, J. L., Berns, A., and Jonkers, J. (2007) Somatic loss of BRCA1 and p53 in mice induces mammary tumors with features of human BRCA1-mutated basal-like breast cancer. *Proc. Natl. Acad. Sci. U.S.A.* **104,** 12111–12116
3. Rottenberg, S., Nygren, A. O., Pajic, M., van Leeuwen, F. W., van der Heijden, I., van de Wetering, K., Liu, X., de Visser, K. E., Gilhuijs, K. G., van Tellingen, O., Schouten, J. P., Jonkers, J., and Borst, P. (2007) Selective induction of chemotherapy resistance of mammary tumors in a conditional mouse model for hereditary breast cancer. *Proc. Natl. Acad. Sci. U.S.A.* **104,** 12117–12122
4. Vollebergh, M. A., Lips, E. H., Nederlof, P. M., Wessels, L. F., Schmidt, M. K., van Beers, E. H., Cornelissen, S., Holtkamp, M., Froklage, F. E., de Vries, E. G., Schrama, J. G., Wesseling, J., van, d., V., van, T. H., de, B. M., Hauptmann, M., Rodenhuis, S., and Linn, S. C. (2010) An aCGH classifier derived from BRCA1-mutated breast cancer and benefit of high-dose platinum-based chemotherapy in HER2-negative breast cancer patients. *Ann. Oncol.* **22,** 1561–1570
5. Silver, D. P., Richardson, A. L., Eklund, A. C., Wang, Z. C., Szallasi, Z., Li, Q., Juul, N., Leong, C. O., Calogrias, D., Buraimoh, A., Fatima, A., Gelman, R. S., Ryan, P. D., Tung, N. M., De Nicolo, A., Ganesan, S., Miron, A., Colin, C., Sgroi, D. C., Ellisen, L. W., Winer, E. P., and Garber, J. E. (2010) Efficacy of neoadjuvant cisplatin in triple-negative breast cancer. *J. Clin. Oncol.* **28,** 1145–1153
6. Derksen, P. W., Braumuller, T. M., van der Burg, E., Hornsveld, M., Mesman, E., Wesseling, J., Krimpenfort, P., and Jonkers, J. (2011) Mammary-specific inactivation of E-cadherin and p53 impairs functional gland development and leads to pleomorphic invasive lobular carcinoma in mice. *Dis. Model. Mech.* **4,** 347–358
7. Cristofanilli, M., Gonzalez-Angulo, A., Sneige, N., Kau, S. W., Broglio, K., Theriault, R. L., Valero, V., Buzdar, A. U., Kuerer, H., Buccholz, T. A., and Hortobagyi, G. N. (2005) Invasive lobular carcinoma classic type: response to primary chemotherapy and survival outcomes. *J. Clin. Oncol.* **23,** 41–48
8. Deans, A. J., and West, S. C. (2011) DNA interstrand cross-link repair and cancer. *Nat. Rev. Cancer* **11,** 467–480
9. Galluzzi, L., Senovilla, L., Vitale, I., Michels, J., Martins, I., Kepp, O., Castedo, M., and Kroemer, G. (2012) Molecular mechanisms of cisplatin resistance. *Oncogene* **31,** 1869–1883
10. Borst, P., Rottenberg, S., and Jonkers, J. (2008) How do real tumors become resistant to cisplatin? *Cell Cycle* **7,** 1353–1359
11. Derksen, P. W., Liu, X., Saridin, F., van der Gulden, H., Zevenhoven, J., Evers, B., van Beijnum, J. R., Griffioen, A. W., Vink, J., Krimpenfort, P., Peterse, J. L., Cardiff, R. D., Berns, A., and Jonkers, J. (2006) Somatic inactivation of E-cadherin and p53 in mice leads to metastatic lobular mammary carcinoma through induction of anoikis resistance and angiogenesis. *Cancer Cell.* **10,** 437–449
12. Warmoes, M., Jaspers, J. E., Pham, T. V., Piersma, S. R., Oudgenoeg, G., Massink, M. P., Waisfisz, Q., Rottenberg, S., Boven, E., Jonkers, J., and Jimenez, C. R. (2012) Proteomics of mouse BRCA1-deficient mammary tumors identifies DNA repair proteins with diagnostic and prognostic value in human breast cancer. *Mol. Cell. Proteomics,* M111.013334
13. Cox, J., and Mann, M. (2008) MaxQuant enables high peptide identification rates, individualized p.p.b.-range mass accuracies and proteome-wide protein quantification. *Nat. Biotechnol.* **26,** 1367–1372
14. Nesvizhskii, A. I., Keller, A., Kolker, E., and Aebersold, R. (2003) A statistical model for identifying proteins by tandem mass spectrometry. *Anal. Chem.* **75,** 4646–4658
15. Keller, A., Nesvizhskii, A. I., Kolker, E., and Aebersold, R. (2002) Empirical statistical model to estimate the accuracy of peptide identifications made by MS/MS and database search. *Anal. Chem.* **74,** 5383–5392

16. Albrethsen, J., Knol, J. C., Piersma, S. R., Pham, T. V., de Wit, M., Mongera, S., Carvalho, B., Verheul, H. M., Fijneman, R. J., Meijer, G. A., and Jimenez, C. R. (2010) Subnuclear proteomics in colorectal cancer: identification of proteins enriched in the nuclear matrix fraction and regulation in adenoma to carcinoma progression. *Mol. Cell. Proteomics* **9,** 988–1005
17. Pham, T. V., Piersma, S. R., Warmoes, M., and Jimenez, C. R. (2010) On the β-binomial model for analysis of spectral count data in label-free tandem mass spectrometry-based proteomics. *Bioinformatics* **26,** 363–369
18. Pham, T. V., and Jimenez, C. R. (2012) An accurate paired sample test for count data. *Bioinformatics* **28,** i596–i602
19. Szklarczyk, D., Franceschini, A., Kuhn, M., Simonovic, M., Roth, A., Minguez, P., Doerks, T., Stark, M., Muller, J., Bork, P., Jensen, L. J., and von Mering, C. (2011) The STRING database in 2011: functional interaction networks of proteins, globally integrated and scored. *Nucleic Acids Res.* **39,** D561–D568
20. Shannon, P., Markiel, A., Ozier, O., Baliga, N. S., Wang, J. T., Ramage, D., Amin, N., Schwikowski, B., and Ideker, T. (2003) Cytoscape: a software environment for integrated models of biomolecular interaction networks. *Genome Res.* **13,** 2498–2504
21. Nepusz, T., Yu, H., and Paccanaro, A. (2012) Detecting overlapping protein complexes in protein-protein interaction networks. *Nat. Methods* **9,** 471–472
22. Maere, S., Heymans, K., and Kuiper, M. (2005) BiNGO: a Cytoscape plugin to assess overrepresentation of gene ontology categories in biological networks. *Bioinformatics* **21,** 3448–3449
23. Rottenberg, S., Jaspers, J. E., Kersbergen, A., van der Burg, E., Nygren, A. O., Zander, S. A., Derksen, P. W., de Bruin, M., Zevenhoven, J., Lau, A., Boulter, R., Cranston, A., O'Connor, M. J., Martin, N. M., Borst, P., and Jonkers, J. (2008) High sensitivity of BRCA1-deficient mammary tumors to the PARP inhibitor AZD2281 alone and in combination with platinum drugs. *Proc. Natl. Acad. Sci. U.S.A.* **105,** 17079–17084
24. Pan, M. R., Hsieh, H. J., Dai, H., Hung, W. C., Li, K., Peng, G., and Lin, S. Y. (2012) Chromodomain helicase DNA-binding protein 4 (CHD4) regulates homologous recombination DNA repair and its deficiency sensitizes cells to poly(ADP-ribose) polymerase (PARP) inhibitor treatment. *J. Biol. Chem.,*
25. Ewing, R. M., Chu, P., Elisma, F., Li, H., Taylor, P., Climie, S., McBroom-Cerajewski, L., Robinson, M. D., O'Connor, L., Li, M., Taylor, R., Dharsee, M., Ho, Y., Heilbut, A., Moore, L., Zhang, S., Ornatsky, O., Bukhman, Y. V., Ethier, M., Sheng, Y., Vasilescu, J., Abu-Farha, M., Lambert, J. P., Duewel, H. S., Stewart, I. I., Kuehl, B., Hogue, K., Colwill, K., Gladwish, K., Muskat, B., Kinach, R., Adams, S. L., Moran, M. F., Morin, G. B., Topaloglou, T., and Figeys, D. (2007) Large-scale mapping of human protein-protein interactions by mass spectrometry. *Mol. Syst. Biol.* **3,** 89
26. Graeser, M., McCarthy, A., Lord, C. J., Savage, K., Hills, M., Salter, J., Orr, N., Parton, M., Smith, I. E., Reis-Filho, J. S., Dowsett, M., Ashworth, A., and Turner, N. C. (2010) A marker of homologous recombination predicts pathologic complete response to neoadjuvant chemotherapy in primary breast cancer. *Clin. Cancer Res.* **16,** 6159–6168
27. Roy, R., Chun, J., and Powell, S. N. (2012) BRCA1 and BRCA2: different roles in a common pathway of genome protection. *Nat. Rev. Cancer* **12,** 68–78
28. Wang, C. H., Wu, H. T., Cheng, H. M., Yen, T. J., Lu, I. H., Chang, H. C., Jao, S. C., Shing, T. K., and Li, W. S. (2011) Inhibition of glutathione *S*-transferase M1 by new gabosine analogues is essential for overcoming cisplatin resistance in lung cancer cells. *J. Med. Chem.* **54,** 8574–8581
29. Vazquez-Martin, A., Colomer, R., Brunet, J., Lupu, R., and Menendez, J. A. (2008) Overexpression of fatty-acid synthase gene activates HER1/HER2 tyrosine kinase receptors in human breast epithelial cells. *Cell Prolif.* **41,** 59–85
30. Uddin, S., Jehan, Z., Ahmed, M., Alyan, A., Al-Dayel, F., Hussain, A., Bavi, P., and Al-Kuraya, K. S. (2011) Overexpression of fatty-acid synthase in Middle Eastern epithelial ovarian carcinoma activates AKT and its inhibition potentiates cisplatin-induced apoptosis. *Mol. Med.* **8,** 635–645
31. Carvalho, M. A., Zecchin, K. G., Seguin, F., Bastos, D. C., Agostini, M., Rangel, A. L., Veiga, S. S., Raposo, H. F., Oliveira, H. C., Loda, M., Coletta, R. D., and Graner, E. (2008) Fatty-acid synthase inhibition with Orlistat promotes apoptosis and reduces cell growth and lymph node metastasis in a mouse melanoma model. *Int. J. Cancer* **123,** 2557–2565
32. Flavin, R., Peluso, S., Nguyen, P. L., and Loda, M. (2010) Fatty-acid synthase as a potential therapeutic target in cancer. *Future Oncol.* **6,** 551–562
33. Mansour, M., Schwartz, D., Judd, R., Akingbemi, B., Braden, T., Morrison, E., Dennis, J., Bartol, F., Hazi, A., Napier, I., and Abdel-Mageed, A. B. (2011) Thiazolidinediones/PPARγ agonists and fatty-acid synthase inhibitors as an experimental combination therapy for prostate cancer. *Int. J. Oncol.* **38,** 537–546
34. Olsen, A. M., Eisenberg, B. L., Kuemmerle, N. B., Flanagan, A. J., Morganelli, P. M., Lombardo, P. S., Swinnen, J. V., and Kinlaw, W. B. (2010) Fatty acid synthesis is a therapeutic target in human liposarcoma. *Int. J. Oncol.* **36,** 1309–1314
35. Uddin, S., Siraj, A. K., Al-Rasheed, M., Ahmed, M., Bu, R., Myers, J. N., Al-Nuaim, A., Al-Sobhi, S., Al-Dayel, F., Bavi, P., Hussain, A. R., and Al-Kuraya, K. S. (2008) Fatty-acid synthase and AKT pathway signaling in a subset of papillary thyroid cancers. *J. Clin. Endocrinol. Metab.* **93,** 4088–4097
36. Uddin, S., Hussain, A. R., Ahmed, M., Bu, R., Ahmed, S. O., Ajarim, D., Al-Dayel, F., Bavi, P., and Al-Kuraya, K. S. (2010) Inhibition of fatty-acid synthase suppresses c-Met receptor kinase and induces apoptosis in diffuse large B-cell lymphoma. *Mol. Cancer Ther.* **9,** 1244–1255
37. Vazquez-Martin, A., Ropero, S., Brunet, J., Colomer, R., and Menendez, J. A. (2007) Inhibition of fatty-acid synthase (FASN) synergistically enhances the efficacy of 5-fluorouracil in breast carcinoma cells. *Oncol. Rep.* **18,** 973–980
38. Zecchin, K. G., Rossato, F. A., Raposo, H. F., Melo, D. R., Alberici, L. C., Oliveira, H. C., Castilho, R. F., Coletta, R. D., Vercesi, A. E., and Graner, E. (2011) Inhibition of fatty-acid synthase in melanoma cells activates the intrinsic pathway of apoptosis. *Lab. Invest.* **91,** 232–240
39. Turrado, C., Puig, T., García-Cárceles, J., Artola, M., Benhamú, B., Ortega-Gutiérrez, S., Relat, J., Oliveras, G., Blancafort, A., Haro, D., Marrero, P. F., Colomer, R., and López-Rodríguez, M. L. (2012) New synthetic inhibitors of fatty-acid synthase with anticancer activity. *J. Med. Chem.* **55,** 5013–5023
40. Puig, T., Aguilar, H., Cufí, S., Oliveras, G., Turrado, C., Ortega-Gutiérrez, S., Benhamú, B., López-Rodríguez, M. L., Urruticoechea, A., and Colomer, R. (2011) A novel inhibitor of fatty-acid synthase shows activity against HER2+ breast cancer xenografts and is active in anti-HER2 drug-resistant cell lines. *Breast Cancer Res.* **13,** R131
41. Puig, T., Turrado, C., Benhamú, B., Aguilar, H., Relat, J., Ortega-Gutiérrez, S., Casals, G., Marrero, P. F., Urruticoechea, A., Haro, D., López-Rodríguez, M. L., and Colomer, R. (2009) Novel inhibitors of fatty-acid synthase with anticancer activity. *Clin. Cancer Res.* **15,** 7608–7615
42. Roodhart, J. M., Daenen, L. G., Stigter, E. C., Prins, H. J., Gerrits, J., Houthuijzen, J. M., Gerritsen, M. G., Schipper, H. S., Backer, M. J., van Amersfoort, M., Vermaat, J. S., Moerer, P., Ishihara, K., Kalkhoven, E., Beijnen, J. H., Derksen, P. W., Medema, R. H., Martens, A. C., Brenkman, A. B., and Voest, E. E. (2011) Mesenchymal stem cells induce resistance to chemotherapy through the release of platinum-induced fatty acids. *Cancer Cell* **20,** 370–383
43. Furuhashi, M., and Hotamisligil, G. S. (2008) Fatty acid-binding proteins: role in metabolic diseases and potential as drug targets. *Nat. Rev. Drug Discov.* **7,** 489–503
44. Nieman, K. M., Kenny, H. A., Penicka, C. V., Ladanyi, A., Buell-Gutbrod, R., Zillhardt, M. R., Romero, I. L., Carey, M. S., Mills, G. B., Hotamisligil, G. S., Yamada, S. D., Peter, M. E., Gwin, K., and Lengyel, E. (2011) Adipocytes promote ovarian cancer metastasis and provide energy for rapid tumor growth. *Nat. Med.* **17,** 1498–1503
45. Mitterberger, M. C., Kim, G., Rostek, U., Levine, R. L., and Zwerschke, W. (2012) Carbonic anhydrase III regulates peroxisome proliferator-activated receptor-γ2. *Exp. Cell Res.* **318,** 877–886
46. Brunet, J., Vazquez-Martin, A., Colomer, R., Graña-Suarez, B., Martin-Castillo, B., and Menendez, J. A. (2008) BRCA1 and acetyl-CoA carboxylase: the metabolic syndrome of breast cancer. *Mol. Carcinog.* **47,** 157–163
47. Wong, R. H., Chang, I., Hudak, C. S., Hyun, S., Kwan, H. Y., and Sul, H. S. (2009) A role of DNA-PK for the metabolic gene regulation in response to insulin. *Cell* **136,** 1056–1072